Computation of Aerodynamic Noise Radiated From Open Propeller Using Boundary Element Method

Jun Huang[1,2]**, Chaopu Zhang**[1]**, Song Xiang**[2]**, Liu Yang**[1]**, Mingxu Yi**[1]

Abstract: In order to accurately predict the aerodynamic noise of the propeller, a hybrid method combining Computational Fluid Dynamics (CFD) method with Boundary Element Method (BEM) is developed in this paper. The calculation includes two steps: firstly, the unsteady viscous flow around the propeller is calculated using the CFD method to acquire the noise source information; secondly, the radiated sound pressure is calculated using BEM method in the frequency domain. In comparison with the experimental results from wind tunnel, the calculated results of aerodynamic performance are rather desirable. The simulation and experimental results of aerodynamic noise are well fitted. The directivity of sound pressure levels (SPLs) of propeller noise is shown in this paper. Simulation shows that the method can effectively calculate aerodynamic noise of the propeller. The acoustic analysis draws some meaningful conclusions.

Keywords: Propeller; Aerodynamic noise; Computational fluid dynamics (CFD); Boundary element method (BEM); SPLs; BPF.

1   Introduction

Aerodynamic propeller is the device which can transform the engine rotational power into thrust of aircraft. Before the advent of the jet engine, the propeller is the driving force device for all of the aircraft with the power. With the continuous development of the technology of the propeller, the noise level and the speed of the aircraft is greatly improved. Propeller-driven aircraft has many advantages, such as low fuel consumption, high flight efficiency, good low speed performance and so on [Hu (2012); Theodorsen (1948); Nelson (1944)]. So the propeller is widely used by regional jet, general aviation and especially unmanned aerial vehicle currently. In addition, the propeller has a wide range of applications in the trainer aircraft, early warning plane, transport aircraft and other models.

---

[1] School of Aeronautic Science and Engineering, Beihang University, Beijing, China
[2] Liaoning Key Laboratory of General Aviation, Shenyang Aerospace University, Shenyang, China

NOMENCLATURE

V	control body	$\boldsymbol{x}$	arbitrary point
∂V	boundary area	$\boldsymbol{y}$	load source point
n	normal vector	p	sound pressure
W	conservation vector	$G(x,y)$	Green function
ρ	density of the fluid	S_j	surface element
u_0, v_0, w_0	projection of absolute velocity in relative coordinate	v	normal velocity on the surface of the blades
E	internal energy of the unit fluid	k	acoustic wave number
H_W, H_V	flux tensors	ω	circular frequency
S_V	source term	c	sound speed
Ω_F	acoustic domain	P_e	predicted pressure
N	number of triangular elements	P_{ref}	reference pressure
N_n	number of nodal points		

Compared with jet propulsion system, noise is obvious drawback of propeller propulsion system. Propeller noise not only influences the surrounding environment of airport, but also induces the structural vibration and acoustic fatigue of aircraft, thereby reducing its safety. So the propeller noise is an important part in the aerodynamic design [Liu (2006); Li (2009)]. The noise is also one of the criterions to measure the propeller performance. The advanced propeller is always developed combining aerodynamic design with aerodynamic acoustics design [Dunn, Tinetti, and Nark (2015)]. With the further understand of noise pollution, reduction the noise produced from open propeller becomes more important. Therefore, investigating the numerical calculation and prediction of aerodynamic noise shows important practical significance.

Aerodynamic noise of the propeller can be divided into rotation noise (discrete noise) and broadband noise. Rotation noise is caused by the periodic interaction between the blades and the flow, and the broadband noise is generated by the random fluctuations of the blade and the surrounding flow. A large number of studies have shown that rotation propeller noise is the main noise of the propeller [Malcolm (1998); Gao and Qiao (2006); Sharma and Chen (2013); Polacsek (2003)]. Rotation noise can be divided into thickness noise, load noise and quadrupole noise. But quadrupole noise shows its importance only when the blade tip works in the transonic and supersonic. For subsonic propeller noise, the main noise consists of thickness noise caused by the monopole source and load noise caused by dipole source. Therefore, we main consider thickness noise and load noise of the propeller in this paper.

Over the last two decades, the Boundary Element Method has become a valuable modeling alternative for several types of engineering problems, especially for problems involving unbounded domains [Chien, Rajiyah, and Atluri (1990); Qian, Han, and Atluri (2004)]. The Boundary Element Method is based on the direct or indirect boundary integral formulation of the considered problem. Compared with the Finite Element Method (FEM), the Boundary Element Method (BEM) involves discretization only of the boundary of the structure and the governing differential equation is solved exactly in the interior, leading to greater accuracy [Qian, Han, and Atluri (2013); Larbi, Deü, Ohayon, and Sampaio (2014); Qian, Han, Ufimtsev, and Atluri (2004)]. Therefore, the Boundary Element Method (BEM) is an ideal analysis tool for problems in acoustics and noise control.

As concerns aerodynamic sound source in blades, many researchers have studied the generation and propagation of the noise of rotor or axial fan or marine propeller, and achieving pretty good results. Generally, the noise source is expressed using acoustic analogy and the flow field is calculated using CFD method [Wang, Luo, and Liu (2003); Xu, Wu, and Chen (2012); Zhang (2009); Wang, Zhao, Xu, Ye, and Wang (2013); Maaloum, Kouidri, and Rey (2004); Lee, Jeon, and Chung (2002)]. Lee, Jeon, and Chung (2002) predicted fan noise using the hybrid method. The flow field is calculated by a vortex method, and acoustic pressures are obtained from the unsteady force fluctuations of the blades using an acoustic analogy. Argüelles, Fernández, Blanco, and Santolaria (2009) investigated the tone noise in a single-stage axial flow fan using the hybrid method, and the propagation of the sound source was predicted using the Ffowcs Williams and Hawkings (FW-H) acoustic analogy. Xia (2014) analyzed the sound radiation of the marine propeller by the direct Boundary Element Method. Hu, Ou, Wu, Jin, Qiang, and Du (2013) studied the rotor–stator interaction noise in axial fans by using a thin-body BEM/Curle method. As the BEM can well predict the noise of the blades, we develop a hybrid method combining Computational Fluid Dynamics (CFD) method with Boundary Element Method (BEM) to predict the aerodynamic noise of the propeller in this paper.

In this paper, The Reynolds-averaged Navier-Stokes (RANS) method and the Boundary Element Method (BEM) are used to predict the noise of propeller. The BEM requires extremely low computational resources, while leading to great accuracy. A method of CFD technique which is based on moving reference frame (MRF) is applied here to investigate the aerodynamics performance of the propeller. The radiated noise of propeller is predicted through solving the Helmholtz equation. The directivity of the sound pressure levels is shown in the research.

2   Governing equations

Due to the rotary speed is constant, in order to study the noise of the propeller, we focus on the flow field in stable state. So the unsteady Navier-Stokes equation is adopted here to calculate the flow field [Li and Xiong (2007)]. In rotating coordinate system, the unsteady Navier-Stokes equation can be expressed as follows

$$\frac{\partial}{\partial t}\iiint_V W\,dV + \oiint_{\partial V} H_W \cdot n\,dA - \oiint_{\partial V} H_V \cdot n\,dA + \iiint_V S_V\,dV = 0 \tag{1}$$

where V is control body, ∂V is the boundary area, n is the normal vector. W is conservation vector, and $W = [\rho, \rho u_0, \rho v_0, \rho w_0, \rho E]^T$, ρ is the density of the fluid, u_0, v_0, w_0 is projection of absolute velocity in relative coordinate, E is the internal energy of the unit fluid. H_W and H_V are the flux tensors. S_V is source term.

Accurate calculation of the flow field is very important for the calculation of sound source. In this paper, the unsteady flow properties are calculated using the commercial CFD code FLUENT 14.0, which has many turbulence models such as $k - \varepsilon$ model, $k - w$ SST model and LES model. The standard $k - \varepsilon$ model is adopted in this paper as its reasonable accuracy and fewer resources in comparison with $k - w$ SST model and LES model. It belongs to the RANS method and the turbulence is considered as isotropic.

3   Boundary element formulation for external acoustic fluid

3.1   *Equations in the frequency domain*

This part presents the direct boundary element method for exterior acoustic fluid in the frequency domain [Larbi, Deü, Ohayon and Sampaio (2014); Xia (2014)]. The governing equations of the acoustic fluid are given as follows:

$$\Delta p + k^2 p = 0 \ \text{ in } \ \Omega_F \tag{2}$$

$$\frac{\partial p}{\partial n} = -i\rho\omega v \tag{3}$$

where Eq. 2 denotes the Helmholtz equation, and k is the acoustic wave number, which is the ratio of the circular frequency ω and the sound speed c.

3.2   *Boundary element formulation*

The boundary element formulation for acoustic problems is valid to the interior and exterior problems. The Helmholtz equation can be used for the pressure p at the arbitrary collocation point x within the acoustic domain Ω_F. A weak form of the

equation is acquired by weighing with the Green function:

$$G(\mathbf{x}, \mathbf{y}) = \frac{e^{ik|\mathbf{x}-\mathbf{y}|}}{4\pi |\mathbf{x}-\mathbf{y}|} \tag{4}$$

where $|\mathbf{x}-\mathbf{y}|$ represents the distance between an arbitrary point $\mathbf{x}$ and the load source point $\mathbf{y}$.

By applying Green's second theorem, the Helmholtz equation can be transformed into the boundary integral equation:

$$c(\mathbf{x})p(\mathbf{x}) = \int_{\partial\Omega_F} p(\mathbf{y}) \frac{\partial G(\mathbf{x}, \mathbf{y})}{\partial n_y} dS - \int_{\partial\Omega_F} \frac{\partial p(\mathbf{y})}{\partial n_y} G(\mathbf{x}, \mathbf{y}) dS \tag{5}$$

where

$$c(\mathbf{x}) = \begin{cases} 1 & \mathbf{x} \text{ in fluid domain} \\ \dfrac{1}{2} & \mathbf{x} \text{ on smooth boundary of fluid domain} \\ \dfrac{\Omega(\mathbf{x})}{4\pi} & \mathbf{x} \text{ on nonsmooth boundary of fluid domain} \\ 0 & \mathbf{x} \text{ outside fluid domain} \end{cases} \tag{6}$$

and

$$\Omega(\mathbf{x}) = 4\pi + \int_{\partial\Omega_F} \frac{\partial \left(|\mathbf{x}-\mathbf{y}|^{-1} \right)}{\partial n_y} dS \tag{7}$$

is the solid angle seen from $\mathbf{x}$. What is notable, $c(\mathbf{x}) = 1/2$ is applied if the surface $\partial\Omega_F$ is supposed to be closed and smooth enough. Generally, the value $c(\mathbf{x}) = \Omega(\mathbf{x})/4\pi$ is accepted when a non-unique tangent plane exists at $\mathbf{x} \in \partial\Omega_F$.

The fluid boundary is divided into N triangular elements ($\partial\Omega_F = \sum_{j=1}^{N} S_j$) and Eq. 5 is discretized. Therefore, for any point x defined by the node i, the discrete Helmholtz equation can be expressed as

$$c_i p_i = \sum_{j=1}^{N} \int_{S_j} p_j(\mathbf{y}) \frac{\partial G(\mathbf{x}_i, \mathbf{y})}{\partial n_y} dS + i\rho\omega \sum_{j=1}^{N} \int_{S_j} v_j(\mathbf{y}) G(\mathbf{x}_i, \mathbf{y}) dS \tag{8}$$

The pressure $p_j(\mathbf{y})$ and the normal velocity $v_j(\mathbf{y})$ can be written as a function of the nodal values of each triangular element j:

$$p_j(\mathbf{y}) = \sum_{k=1}^{3} N_k p_j^k = \mathbf{N}\mathbf{p}_j, v_j(\mathbf{y}) = \sum_{k=1}^{3} N_k v_j^k = \mathbf{N}\mathbf{v}_j \tag{9}$$

and Eq. 8 is transformed into

$$c_i p_i = \sum_{j=1}^{N} \sum_{k=1}^{3} \int_{S_j} N_k \frac{\partial G(\boldsymbol{x}_i, \boldsymbol{y}_j)}{\partial n_y} dS p_j^k + i\rho\omega \sum_{j=1}^{N} \sum_{k=1}^{3} \int_{S_j} N_k G(\boldsymbol{x}_i, \boldsymbol{y}_j) dS v_j^k \tag{10}$$

or the following form

$$c_i p_i = \sum_{j=1}^{N} \sum_{k=1}^{3} H_{ij}^k p_j^k + i\rho\omega \sum_{j=1}^{N} \sum_{k=1}^{3} G_{ij}^k v_j^k \tag{11}$$

where

$$H_{ij}^k = \int_{S_j} N_k \frac{\partial G(\boldsymbol{x}_i, \boldsymbol{y}_j)}{\partial n_y} dS \quad G_{ij}^k = \int_{S_j} N_k G(\boldsymbol{x}_i, \boldsymbol{y}_j) dS \tag{12}$$

Placing point $\boldsymbol{x}_i$ at each nodal point on the boundary $\boldsymbol{y}_j$ in succession, we can obtain

$$c_i \delta_{ij} p_j = \sum_{j=1}^{N} \sum_{k=1}^{3} H_{ij}^k p_j^k + i\rho\omega \sum_{j=1}^{N} \sum_{k=1}^{3} G_{ij}^k v_j^k \tag{13}$$

By repeating the collocation scheme for all nodal points N_n of the boundary element mesh, a set of N_n expressions is then obtained in the nodal field variables, which can be assembled into the following matrix equation:

$$\boldsymbol{HP} = i\rho\omega\boldsymbol{G}v \tag{14}$$

where $\boldsymbol{P}$ denotes the vector with sound pressure, and $\boldsymbol{v}$ denotes the vector with velocity in the normal direction to the boundary surface at the nodal position of the boundary element mesh.

In this paper, through solving the matrix equation, we try to realize the numerical prediction of propeller noise.

4 Numerical results and discussions

4.1 Geometric configuration and grid generation

In this part, a high efficiency propeller is used to demonstrate the effectiveness of the present method. The experimental propeller is a composed of 2 blades and has a maximum chord length of 17mm and total span of 960mm. The sketch of the experimental propeller is shown in Fig. 1.
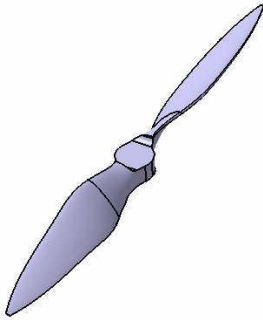
Figure 1: Sketch of the experimental propeller.
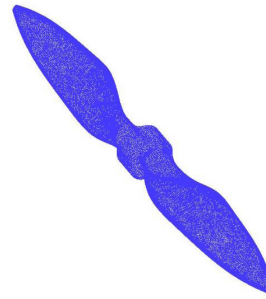
Figure 2: Meshes on propeller surfaces.

The propeller surface is constructed by triangle mesh, as shown in Fig. 2. The experimental propeller geometry is embedded in a columniform domain which is shown in Fig. 4. In this study, the computational domain is divided into an independent rotational domain for the experimental propeller and an outer stationary domain, with the former made up of refined, unstructured tetrahedral volumes(shown in Fig. 2–3), while the latter-the far-field blocks composed of structured hexahedra(shown in Fig. 4). The grid in the leading edge and trailing edge of the experimental propeller adopts the adaptive encryption technique. Considering the inlet and outlet zone, the total number of cells in the whole flow field is about 3.6 million.
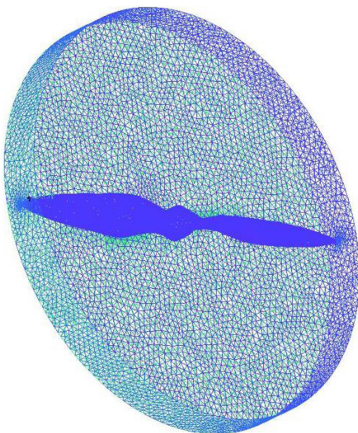
Figure 3: Rotation domain.

Figure 4: Structured quadrilateral for the far-field.

4.2   Aerodynamic performance of the propeller

The flow simulation is carried out by the Reynolds Averaged Navier–Stokes equation which is supplied in Fluent. The boundary conditions are set as follows: velocity-inlet for inlet zone, outlet-vent for outlet zone, wall on propeller, and matching interface. First, the numerical solution is obtained by moving reference frame model. Then in order to acquire the final solution of the flow, the approximation is restarted with the sliding mesh. The solution domain is divided into two parts of rotating and static by a cylinder whose diameter equals the propeller's diameter and length equals the propeller's height. In order to keep the information of the unsteady flow, interfaces are set between two parts to carry on the information interchange of the physical quantity. And the propeller is represented by the no-slip wall. The no-slip wall allows viscous effects at the faces of the propeller and leads to the formation of a boundary layer, so the no-slip wall can represent the real world situation. In this paper, the standard $k - \varepsilon$ turbulence model is used to calculate the simulation. The SIMPLEC discretization schemes were adopted to discretize the equations of pressure–velocity coupling. And finally the second order discretization scheme was used here, because it is the best choice here for the simulation though the current investigation.

The pressure nephograms of the propeller at different rotary speed and flight speed are shown in Fig. 5–7, respectively. The pressure nephograms above show that the pressure at the leading edge of the propeller is higher than the trailing edge's.

The calculated results of the propeller's tension on Z axis at different rotary speed and flight speed are shown in the Tab. 1. Tab. 1 also presents experimental results
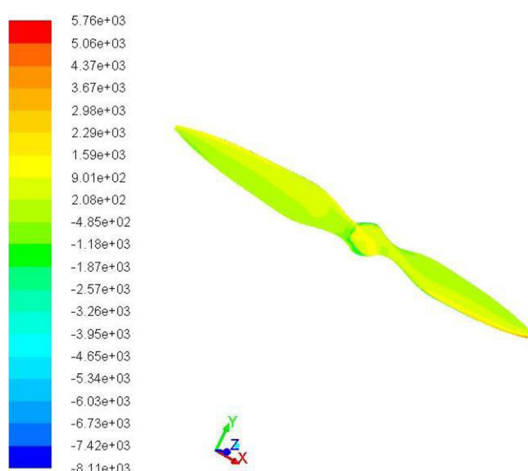
Figure 5: Pressure distribution of the propeller at 900rpm.
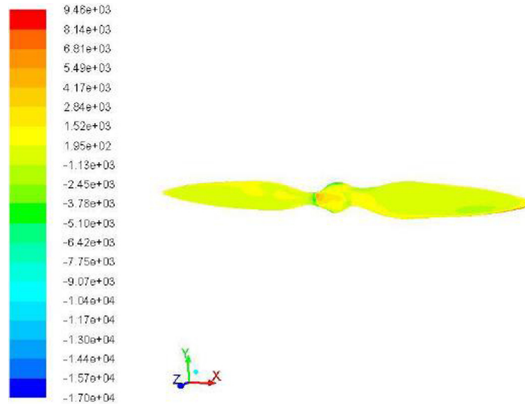
Figure 6: Pressure distribution of the propeller at 1800rpm.
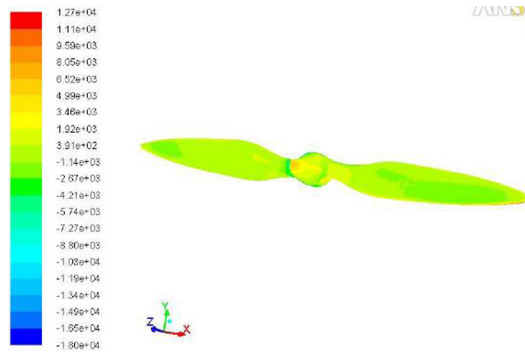
Figure 7: Pressure distribution of the propeller at 2100rpm.

Table 1: The comparison of experimental results and calculated results of propeller's tension on *Z* axis.

Rotary speed (rpm)	Flight speed (m/s)	Experimental results (N)	Calculated results (N)
900	30.74	−46.3	−43
1800	30.74	−7.7	−10
2100	30.75	33.6	29

obtained by the wind tunnel. Compared with experimental results of the wind tunnel, we can confirm that the CFD method is rather desirable. The results show that this method can investigate aerodynamic performance of the propeller effectively.

4.3   *Aerodynamic noise of the propeller*

In this part, the acoustic calculation and analysis are shown. For subsonic propeller noise, the main noise consists of thickness noise caused by the monopole source and load noise caused by dipole source. So we calculate these two noises in this paper.
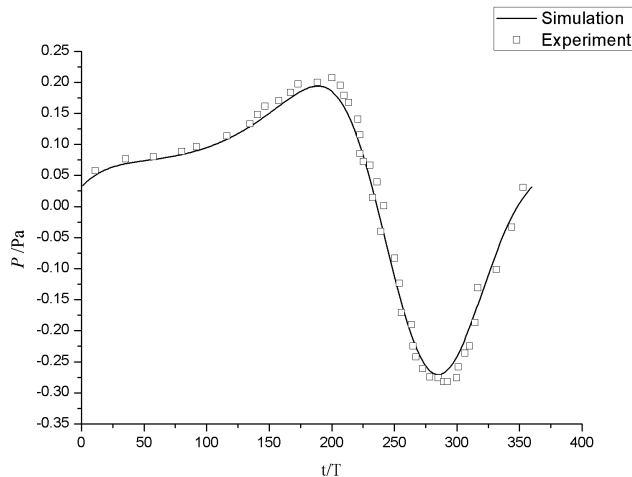
Figure 8: Simulation and experimental results of sound pressure of the propeller at 900rpm.
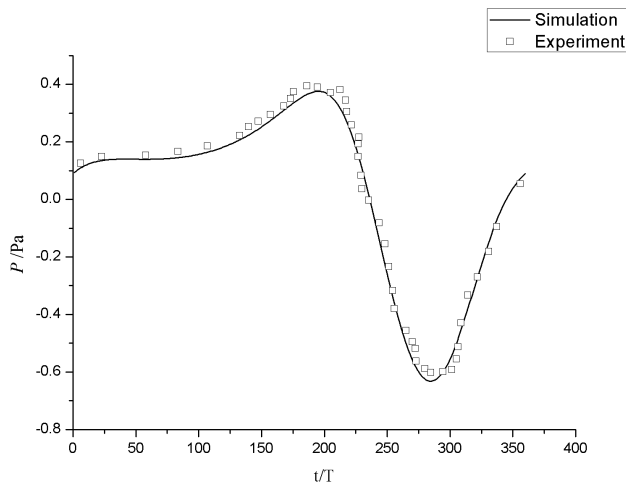
Figure 9: Simulation and experimental results of sound pressure of the propeller at 1200rpm.

The simulation and experimental results of sound pressure of the propeller at 5R (R denotes the radius of the propeller) at different rotary speeds are shown in Fig. 8-9, respectively. In comparison with the experimental results, we find the hybrid method can simulate aerodynamic noise of the propeller very well.

In order to do some research on the characteristic of aerodynamic noise of the propeller, we define a circle which is 5R or 10R radius to calculate the directivity of the SPLs. The center of the circle is at the position of the propeller, and a number of observer points 1 degree intervals are set along the circle.
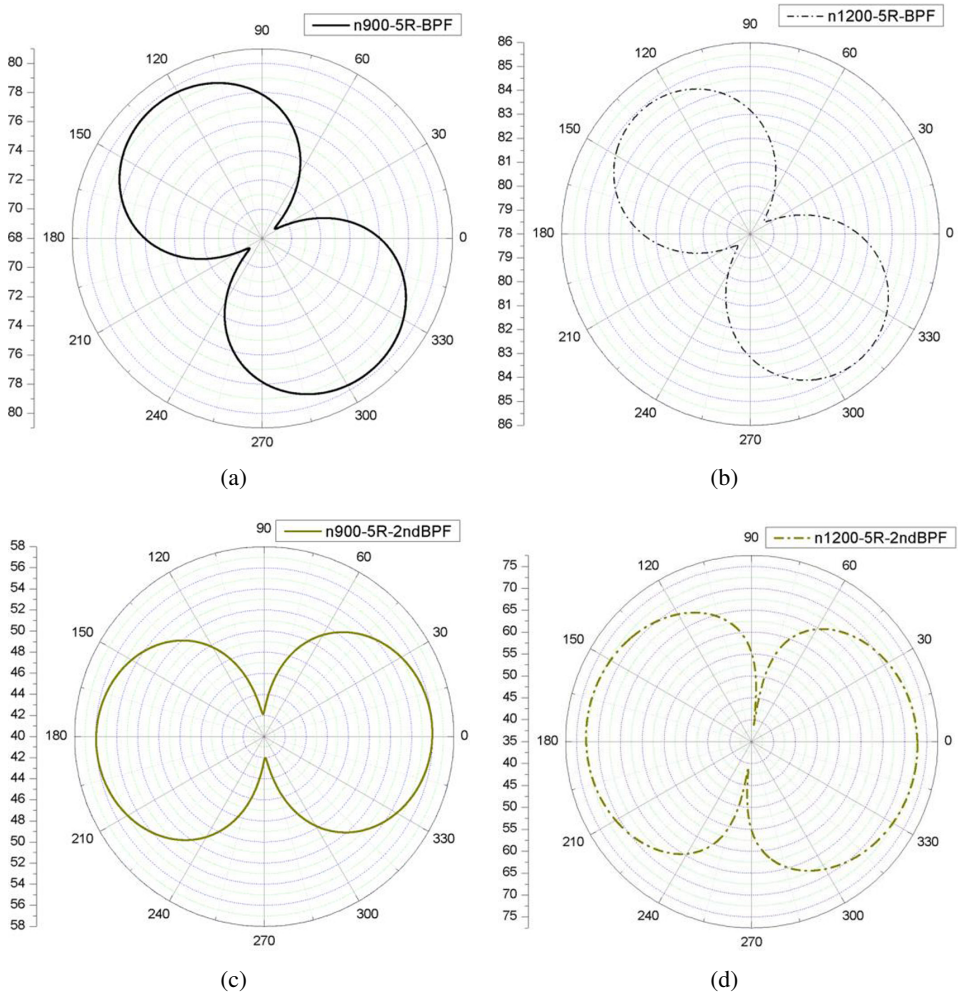
Figure 10: Directivity of the propeller noise SPLs in BPF and its harmonics for different rotary speed.

As the parameters of the force need to be used in frequency domain, the time-dependent components of the force on the propeller are transformed using Fast Fourier Transformation (FFT) method. The sound pressure is expressed in decibels (dB) and the unweighted sound pressure level (SPL) is calculated using the following equation:

$$SPL = \frac{P_e}{P_{ref}} \tag{15}$$

where P_e represents the predicted pressure, P_{ref} represents the reference pressure and $P_{ref} = 2 \times 10^{-5} Pa$.

The directivity of the propeller noise SPLs in BPF and its harmonics for different rotary speeds are shown in Fig. 10, the left rotary speed is 900rpm and the right is 1200rpm at the observation distance of 5R (R denotes the radius of the propeller).The results show that the SPLs of the propeller at BPF will increase simultaneously when the rotary speed increase. The same conclusion can be conducted with its harmonics.

The directivity of the propeller noise SPLs in BPF and its harmonics for different observation distances are shown in Fig. 11. The different observation distances are 5R and 10R at the rotary speed of 1200rpm, respectively. We can conclude that the SPLs of the propeller in BPF will decrease obviously with the increase of observation distance. The same conclusion can be conducted with its harmonics.
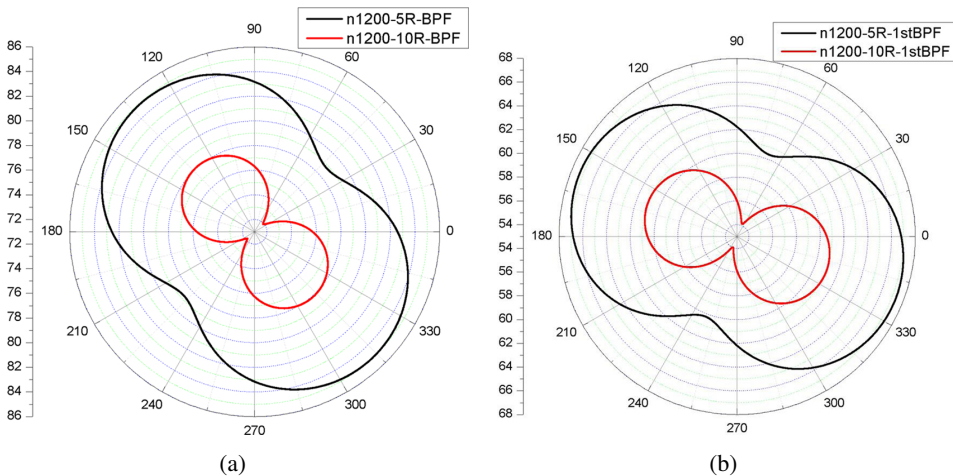
Figure 11: Directivity of the propeller noise SPLs in BPF and its harmonics for different observation distance.

(a)

(b)

(c)
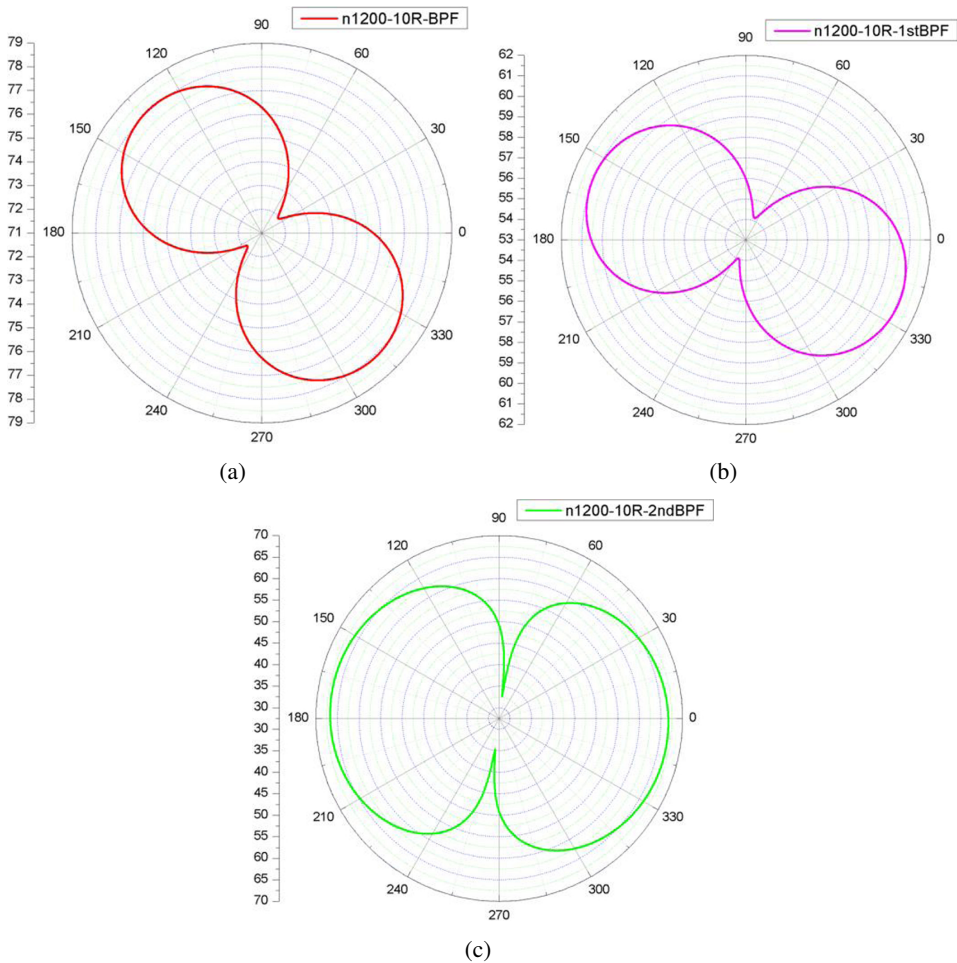
Figure 12: Directivity of the propeller noise SPLs in BPF, 1stBPF and 2nd BPF.

The directivity of the propeller noise SPLs in BPF and its harmonics (1stBPF and 2nd BPF) are presented in Fig. 12. The rotary speed is 1200rpm at 10R. We can find that the SPLs of the propeller in BPF are higher than its harmonics'. The same conclusion can be conducted with other speed at any observation distance.

5 Conclusion

In this paper, the hybrid method combining CFD method with Boundary Element Method (BEM) was applied to calculate the aerodynamic noise of propeller. The Reynolds-averaged Navier-Stokes (RANS) numerical calculation was used to acquire the properties of the unsteady flow. The unsteady force of the propeller was

obtained from the unsteady numerical results, and the pressure data was used to calculate the sound source. The Boundary Element Method (BEM) can effectively predict the propeller noise. The result showed that the SPLs of the propeller in BPF and its harmonics increase with the increase of the rotary speed, while decrease with the increase of observation distance. The results also showed that the SPLs of the propeller in BPF are higher than its harmonics'.

References

Argüelles, Díaz. K. M.; Fernández, O. J. M.; Blanco, M. E.; Santolaria, M. C. (2009): Numerical prediction of tonal noise generation in an inlet vaned low-speed axial fan using a hybrid aeroacoustic approach. *Proc IMechE, Part C: J Power Energy*, vol. 221, pp. 2081–2098.

Chien, C. C.; Rajiyah, H.; Atluri, S. N. (1990): An effective method for solving the hyper-singular integral equations in 3-D acoustics. *Journal of the Acoustical Society of America*, vol. 88, no. 2, pp. 918–937.

Dunn, M.; Tinetti, A.; Nark, D. (2015): Open rotor noise prediction using the time domain formulations of Farassat. *International Journal of Aeroacoustics*, vol. 14, no. 1–2, pp. 51–86.

Gao, Y. W.; Qiao, Z. D. (2006): A fast numerical method for calculating propeller aerodynamic and acoustic characteristics. *Acta Aerodynamica Sinica*, vol. 24, no. 2, pp. 187–193.

Hu, B. B.; Ou, Y. H.; Wu, Y. D.; Jin, G. Y.; Qiang, X. Q.; Du, Z. H. (2013): Numerical prediction of the interaction noise radiated from an axial fan. *Applied Acoustics*, vol. 74, no. 4, pp. 544–552.

Hu, Y. (2012): *CFD simulation of propeller performance and the influence of slipstream flow*. Nanjing University of Aeronautics and Astronautics.

Larbi, W.; Deü, J.-F.; Ohayon, R.; Sampaio, R. (2014): Coupled FEM/BEM for control of noise radiation and sound transmission using piezoelectric shunt damping. *Applied Acoustics*, vol. 86, pp. 146–153.

Lee, D. J.; Jeon, W. H.; Chung, K. H. (2002): Development and application of fan noise prediction method to axial and centrifugal fan. *In: Proceedings of FEDSDL2002-60265, ASME joint US-European fluids engineering conference*, pp. 987–992.

Li, P. (2009): The analysis of aircraft propeller noise and decreasing. *Equipment Manufacturing Technology*, vol. 8, pp. 37–38.

Li, X. H.; Xiong, J. J. (2007): On navier-stokes equation-based aerodynamic interaction between rotor blades in hover phase. *Acta Aerodynamica Sinica*, vol. 25, no. 2, pp. 271–276.

Liu, P. Q. (2006): *Air propeller theory and its application.* Beijing: Beihang University Press.

Maaloum, A.; Kouidri, S.; Rey, R. (2004): Aeroacoustic performance evaluation of axial flow fans based on the unsteady pressure field on the blade surface. *Applied Acoustics*, vol. 65, no. 4, pp. 367–384.

Malcolm, J. C. (1998): *Handbook of acoustics*. John Wiley & Sons.

Nelson, W. C. (1944): *Airplane propeller principles.* J. Wiley & Sons, inc.

Polacsek, C. (2003): Fan interaction noise reduction using a wake generator: experiments and computational aeroacoustics. *Journal of Sound and Vibration*, vol. 265, pp. 725–743.

Qian, Z. Y.; Han, Z. D.; Atluri, S. N. (2013): A fast regularized boundary integral method for practical acoustic problems. *CMES: Computer Modeling in Engineering & Sciences*, vol. 91, no. 6, pp. 463–484.

Qian, Z. Y.; Han, Z. D.; Atluri, S. N. (2004): Directly derived non-hyper-singular boundary integral equations for acoustic problems, and their solution through Petrov-Calerkin schemes. *CMES: Computer Modeling in Engineering & Sciences*, vol. 5, no. 6, pp. 541–562.

Qian, Z. Y.; Han, Z. D.; Ufimtsev, P.; Atluri, S. N. (2004): Non-hyper-singular boundary integral equations for acoustic problems, implemented by the collocation-based boundary element method. *CMES: Computer Modeling in Engineering & Sciences*, vol. 6, no. 2, pp. 133–144.

Sharma, A.; Chen, H. (2013): Prediction of aerodynamic tonal noise from open rotors. *Journal of Sound and Vibration*, vol. 332, no. 16, pp. 3832–3845.

Theodorsen, T. (1948): *Theory of propellers.* New York: McGraw-hill.

Wang, B.; Zhao, Q. J.; Xu, G. H.; Ye, L.; Wang, J. Y. (2013): Numerical analysis on noise of rotor with unconventional blade tips based on CFD/Kirchhoff method. *Chinese Journal of Aeronautics*, vol. 26, no. 3, pp. 572–582.

Wang, Z. H.; Luo, B. H.; Liu, Y. L. (2003): Numerical methods and advances for aeroacoustics. *Chinese Quarterly of Mechanics*, vol. 24, no. 2, pp. 219–225.

Xia, P. P. (2014): *The design strategy of low noise propeller*. Harbin Institute of Technology.

Xu, J. W.; Wu, Y. F.; Chen, G. (2012): Comparison and application on the aeroacoustics numerical computing methods. *Noise and Vibration Control*, vol. 4, pp. 6–10.

Zhang, J. M. (2009): *Research of numerical method for computational aeroacoustics*. Nanjing University of Aeronautics and Astronautics.